



# On the cooling of a deep terrestrial magma ocean



J. Monteux<sup>a,\*</sup>, D. Andrault<sup>a</sup>, H. Samuel<sup>b</sup>

<sup>a</sup> Laboratoire Magmas et Volcans, Université Blaise Pascal, CNRS, IRD, Clermont-Ferrand, France

<sup>b</sup> Institut de Recherche en Astrophysique et Planétologie, CNRS, Toulouse, France

## ARTICLE INFO

### Article history:

Received 18 November 2015  
 Received in revised form 21 April 2016  
 Accepted 7 May 2016  
 Available online 24 May 2016  
 Editor: C. Sotin

### Keywords:

early Earth  
 thermal evolution  
 magma ocean  
 numerical modeling

## ABSTRACT

Several episodes of complete melting have probably occurred during the first stages of the Earth's evolution. We have developed a numerical model to monitor the thermal and melt fraction evolutions of a cooling and crystallizing magma ocean from an initially fully molten mantle. For this purpose, we numerically solve the heat equation in 1D spherical geometry, accounting for turbulent heat transfer, and integrating recent and strong experimental constraints from mineral physics. We have explored different initial magma ocean viscosities, compositions, thermal boundary layer thicknesses and initial core temperatures.

We show that the cooling of a thick terrestrial magma ocean is a fast process, with the entire mantle becoming significantly more viscous within 20 kyr. Due to the slope difference between the adiabats and the melting curves, the solidification of the molten mantle occurs from the bottom up. In the meantime, a crust forms due to the high surface radiative heat flow, the last drop of fully molten silicate is restricted to the upper mantle. Among the studied parameters, the magma ocean lifetime is primarily governed by its viscosity. Depending on the thermal boundary layer thickness at the core–mantle boundary, the thermal coupling between the core and magma ocean can either insulate the core during the magma ocean solidification and favor a hot core or drain the heat out of the core simultaneously with the cooling of the magma ocean. Reasonable thickness for the thermal boundary layer, however, suggests rapid core cooling until the core–mantle boundary temperature results in a sluggish lowermost mantle. Once the crystallization of the lowermost mantle becomes significant, the efficiency of the core heat loss decreases. Since a hotter liquidus favors crystallization at hotter temperatures, a hotter deep mantle liquidus favors heat retention within the core. In the context of an initially fully molten mantle, it is difficult to envision the formation of a basal magma ocean or to prevent a major heat depletion of the core. As a consequence, an Earth's geodynamo sustained only by core cooling during 4 Gyr seems unlikely and other sources of motion need to be invoked.

© 2016 Elsevier B.V. All rights reserved.

## 1. Introduction

Geochemical evidence (Touboul et al., 2012; Rizo et al., 2013) suggests that the Earth's mantle has experienced several episodes of global melting during its early evolution, leading to the formation of the early continental crust and facilitating the core formation (Kleine et al., 2009). These episodes were probably enhanced by giant impacts occurring during the late stages of planetary formation (Agnor et al., 1999). Although not yet clearly established, it is likely that these giant impacts, such as the one that is thought to have formed the Earth–Moon system, could have melted 30 to 100% of the Earth's mantle depending on the impactor/target mass ratio and on the pre-impact ther-

mal state of the target (Canup, 2012; Čuk and Stewart, 2012; Nakajima and Stevenson, 2015). During the cooling and the subsequent crystallization of a magma ocean (MO), compatible elements (e.g. Mg, Cr) were preferentially collected in the solid phase while the incompatible elements (e.g. Al, Na, Fe) selectively partitioned into melts. In addition to temperature, the degree of solid–melt fractionation is highly sensitive to a variety of physical parameters, including pressure (Nomura et al., 2011; Andrault et al., 2012). Hence, characterizing the cooling of a deep terrestrial magma ocean and in particular the timescale and depth at which the last drop of melt solidifies are of first importance to understand the current chemical composition of the Earth's mantle and the dating of its major differentiation events (Boyet and Carlson, 2005).

The composition and the rheology of such a magma ocean directly affect its lifetime, but remain poorly constrained (Solomatov, 2007). The magma ocean is composed of low viscosity molten sili-

\* Corresponding author.

E-mail address: j.monteux@opgc.univ-bpclermont.fr (J. Monteux).

cate material but its chemical composition remains uncertain, with a MgO/SiO<sub>2</sub> ratio around those of chondritic or peridotitic compositions (Ringwood, 1966; Allègre et al., 1995; Javoy et al., 2010). Recent high-pressure laboratory measurements report the solidus and liquidus of both a chondritic and peridotitic mantle compositions up to pressures that are compatible with the Earth's lowermost mantle conditions (Fiquet et al., 2010; Andraut et al., 2011). Moreover, recent shock experiments now provide important constraints on the thermodynamic parameters used to determine the adiabatic profiles in the magma ocean up to 140 GPa (Mosenfelder et al., 2009; Thomas et al., 2012; Thomas and Asimow, 2013). Since the difference between their slopes governs the depth at which crystallization is initiated, both the liquidus and the adiabats play a key role in the cooling of the magma ocean. If the adiabat had a steeper slope than the liquidus in the mid-mantle (Mosenfelder et al., 2007; Stixrude et al., 2009), solidification would start at mid-mantle depth. In this case, a lowermost magma ocean would cool and solidify much more slowly because of the thermal blanketing of the overlying solid mantle (Labrosse et al., 2007). However, if the mantle liquidus had a steeper slope than the adiabat through the whole mantle (Thomas et al., 2012), solidification would start from the CMB thus reducing the likeliness of a basal magma ocean, unless invoking an enrichment in dense incompatible elements in the residual liquid. In any case, the important dynamical change does not occur when the adiabat crosses the liquidus, because the mantle keeps its liquid behavior, but rather when the degree of partial melting decreases below a critical value from which the mantle behaves as a solid. Therefore, the recent determination of melting curves and elastic parameters of silicate melts up to core–mantle boundary (CMB) conditions offers a great opportunity to improve our knowledge of the cooling dynamics of a deep terrestrial magma ocean.

The magma oceans such as the one generated by the Moon-forming impact participated to the core-formation process. The early thermal state of the core remains poorly constrained. It results from the contribution of the accretionary processes (Safronov, 1978; Kaula, 1979), including giant impact (Tonks and Melosh, 1992) and radiogenic heating (Yoshino et al., 2003) as well as the conversion of potential energy into heat via viscous dissipation during the metal/silicate separation (Ke and Solomatov, 2009; Monteux et al., 2009; Ricard et al., 2009; Samuel et al., 2010). The combined processes leading to core formation can yield a wide range of possible early thermal states, depending on the nature and timescale of core formation processes. The core could initially have had a temperature close to the deep mantle temperature if thermal equilibration was efficient. Alternatively, it could have been hotter than the mantle if the gravitational potential energy released during core formation was largely retained within the core itself, a situation which would be followed by a strong heating of the lowermost mantle from this superheated core (Samuel et al., 2010). In turn, the thermo-mechanical properties of the magma ocean can have a strong influence on the early evolution of the heat repartition between the core and the mantle. A key question is to determine how much a deep magma ocean can enhance core cooling. This can have important consequences on the duration and the generation of the Earth's dynamo (Monteux et al., 2011).

The low magma ocean viscosities resulting from the hot early temperatures imply that the cooling of such a deep molten mantle was highly turbulent (Solomatov, 2007). Studies of the early mantle have either characterized the cooling of a magma ocean restricted to the first 1000 km (Abe, 1997) or did not consider the presence of a molten layer just above the core–mantle boundary, and its effect of the CMB heat flow (Nakagawa and Tackley, 2014). However, the hypothesis of an early largely molten mantle combined with the determination of solidus/liquidus and thermodynamical properties of silicate melts up to 140 GPa now allow a more accurate

characterization of the cooling of a deep terrestrial magma ocean and the thermal coupling with its underlying core. The aim of this work is to constrain the lifetime of a deep magma ocean and to determine the pressure at which the magma ocean crystallization finished. To achieve these goals, we have developed a numerical model to characterize the early evolution of (i) the temperature and melt fraction of an initially fully molten isochemical mantle and (ii) the temperature of the core. We incorporate in our models recent and strong experimental constraints on the solidus and liquidus profiles and on the thermodynamical properties of silicate melts up to ~140 GPa. We explore different core temperatures, magma ocean compositions and viscosities.

## 2. Convective cooling of the magma ocean

Miller et al. (1991) characterized the cooling and the subsequent crystallization of a magma ocean with a chondritic composition as a sequence of isentropes with decreasing potential temperature. Later on, Abe (1997) investigated the thermal evolution of magma ocean using a one-dimensional heat transfer model. However, these studies were restricted to the first 1000 km and did not integrate the mutual influence of the magma ocean and its underlying material on the cooling. Labrosse et al. (2007) studied the cooling of a stable dense molten layer above the CMB overlaid by a solid mantle. In their model they consider the crystallization of a single-component (forsterite) magma ocean assuming a solidification proceeding from the top to the bottom according to Mosenfelder et al. (2007). More recently, Nakagawa and Tackley (2014) characterized the coupled thermal evolution of Earth's early mantle and core considering a 2900 km thick viscous mantle but ignoring the potential presence of a molten layer just above the core–mantle boundary, and its effect of the CMB heat flow. Here, we model the secular cooling of an initially fully molten magma ocean by convective transport of heat in a 1-D spherically symmetric geometry. We assume a multicomponent chemically homogeneous magma ocean made of a combination of forsterite, enstatite, fayalite, anorthite and diopside. In the following sections, we describe the model setup and equations.

### 2.1. Physical model for planetary thermal evolution

We model the thermal evolution of a 2900 km thick isochemical silicate mantle overlying an iron core by solving the conservation of energy in a one-dimensional, spherically symmetric domain (with a radius ranging from 3500 to 6400 km):

$$\rho C_p \frac{\partial T}{\partial t} = \nabla \cdot (k \nabla T), \quad (1)$$

with  $\rho$  the density,  $C_p$  the mantle heat capacity,  $T$  the temperature,  $t$  the time and  $k$  the thermal conductivity. Among the heat sources that have potentially delivered the energy required for significant melting in the early Earth, the decay of short-lived radioactive isotopes such as <sup>26</sup>Al and <sup>60</sup>Fe have probably played a major role especially for 10 to 100 km size objects (Yoshino et al., 2003). However, their half-life times (0.73 My and 1.5 My respectively) (Carlson and Lugmair, 2000) are much shorter than the time at which the Moon forming impact is supposed to have occurred (between 30 and 100 Myrs after the formation of the first solids of the Solar System) (Kleine and Rudge, 2011). Concerning the long-lived radioactive elements such as <sup>40</sup>K, Th or U, their concentrations were certainly significant at the time of the Moon-forming impact, but their heat production rates are much smaller. Hence the contribution from the long-lived radio-active elements during the magma ocean lifetime is negligible. Thus, we can reasonably neglect radiogenic heating in our models.

Thermal energy is transferred by convection in the region where the temperature gradient is steeper than the adiabatic temperature gradient, or by conduction elsewhere. To account for the heat transfer within a vigorously convecting magma ocean, in Eq. (1), the thermal conductivity  $k$  is the sum of the intrinsic thermal conductivity  $k_c$  and an effective conductivity due to thermal convection  $k_v$ . Following Neumann et al. (2014), the latter is estimated as follows:

$$k_v = F_{conv}L/\Delta T, \quad (2)$$

where  $L$  is the thickness of the magma ocean at time  $t$ ,  $F_{conv}$  is the convective heat flux at radius  $r$  and time  $t$  and  $\Delta T$  is the difference between the temperature profile and the adiabatic profile  $T_{ad}$  with a potential temperature corresponding to the temperature of the surface of the magma ocean.

At radius  $r$ , the convective heat flux  $F_{conv}$  depends on the local Rayleigh number  $Ra$ :

$$Ra = \frac{\alpha g C_p \rho^2 \Delta T L^3}{k_c \eta}, \quad (3)$$

where  $\alpha$  is the thermal expansion coefficient of the magma ocean,  $g$  is the gravitational acceleration assumed to be constant through the whole mantle and  $\eta$  is the local dynamic viscosity.

In the context of an initially fully molten mantle, the convective velocities are estimated to  $u_0 \sim 10$  m/s (Solomatov, 2007) leading to Reynolds number values ( $Re = \rho u_0 L / \eta$ ) in the order of  $10^9$  (with  $\eta = 100$  Pa s and  $\rho = 4000$  kg m<sup>-3</sup>) and, hence, to highly turbulent convective cooling. The low magma ocean viscosities induce Rayleigh numbers as large as  $10^{30}$  (Solomatov, 2007). In such a context, two regimes arise depending on  $Ra$  (Solomatov, 2007; Neumann et al., 2014): the “soft-turbulent” regime (if  $Ra < 10^{19}$ ) where

$$F_{conv} = 0.089 \frac{k_c \Delta T}{L} Ra^{1/3}, \quad (4)$$

and the “hard-turbulent” regime (if  $Ra \geq 10^{19}$ ) where

$$F_{conv} = 0.22 \frac{k_c \Delta T}{L} Ra^{2/7} Pr^{-1/7} \lambda^{-3/7}, \quad (5)$$

where  $Pr$  is the local Prandtl number ( $= C_p \eta / k_c$ ) and  $\lambda$  is the aspect ratio for the mean flow. We assume that  $\lambda = 1$  and that rotation does not have any significant effect on the heat flow (Solomatov, 2007).

Depending on their ability to migrate either towards the solid phase (compatible) or towards the liquid phase (incompatible), the relative abundance of some chemical elements can potentially modify the buoyancy of both the liquid and solid phases during the crystallization of a magma ocean. This chemical fractionation process could be enhanced by the fractional crystallization of the magma ocean at least in the upper mantle (Solomatov, 2007) and would lead to a liquid residual phase that is more or less buoyant than the solid phase. A dense liquid phase could favor a basal magma ocean (Labrosse et al., 2007) or large scale cumulate overturns (Elkins-Tanton et al., 2003, 2005) while a dense solid phase would enhance volcanic activity (Moyen and Martin, 2012; Martin et al., 2014). However, the values of the partition coefficients at high pressures of the elements that have a key contribution in the density of each phase (e.g. Fe) are still debated (Andraut et al., 2012). In addition, crystals may also gravitationally separate with the dense cumulates sinking and the lighter ones floating toward the surface leading to a supplementary segregation process. In a highly turbulent environment such as a thick magma ocean, the vigor of the convection probably prevents from any chemical segregation especially during the early stages of the magma ocean solidification. Indeed, Tonks and Melosh (1990) have

shown that the Rayleigh number for a planetary scale magma ocean was so high that crystals would remain entrained in the magma which would effectively preclude crystal separation. Therefore, we do not consider any spatial variation in the chemical composition and we currently consider neither the mass flux of melt owing to gravitational separation nor the mass flux of melt owing to convective mixing.

Viscosity is strongly dependent on the local melt fraction  $\phi$ , which is calculated as follows:

$$\phi = \frac{T - T_{sol}}{T_{liq} - T_{sol}}, \quad (6)$$

where  $T_{liq}$  and  $T_{sol}$  are the liquidus and solidus temperatures, respectively. Following Abe (1997) the viscosity of partially molten silicates  $\eta$  varies between a fully molten end-member  $\eta_m$  (assumed to be constant) and a solid end-member  $\eta_s$  that is temperature dependent:

$$\eta = \text{MIN} \left[ \frac{(1 - \phi) \rho_m \eta_s + \phi \rho_s \eta_m}{(1 - \phi) \rho_m + \phi \rho_s}, \eta_m \left\{ \frac{(1 - \phi) \rho_m + \phi \rho_s}{(1 - A)(1 - \phi) \rho_m + \phi \rho_s} \right\}^{2.5}, 10^{21} \right], \quad (7)$$

where  $\rho_m$  is the density of the molten material,  $\rho_s$  is the density of the solid material and  $A = 1.67$  (Abe, 1997). When the temperature,  $T$ , is lower than the solidus temperature of mantle, the viscosity of the solid mantle  $\eta_s$  is estimated as follows (Abe, 1997):

$$\eta_s = \eta_{s,0} \exp \left( B \frac{T_{liq}}{T} \right). \quad (8)$$

We used  $\eta_{s,0} = 256$  Pa s, and  $B = 25.17$  based on the olivine rheology (Karato and Wu, 1993; Abe, 1997). In the above equation, as for an Arrhenius relation, the viscosity of the solid mantle increases with the pressure. Assuming an adiabatic temperature profile with a potential temperature of 1600 K (Tackley, 2012) leads to a viscosity value of  $\sim 10^{23}$  Pa s in the lowermost mantle compatible with estimates of the present-day mantle viscosity profiles (Čížková et al., 2012). Considering a relationship that involves the solidus rather than the liquidus in Eq. (8) would not affect our results since both the liquidus and the solidus used in our models have a similar trend. Since we consider here the evolution of a fully molten to partially molten magma ocean, the cooling timescale of the magma ocean is mainly governed by  $\eta_m$  and is weakly dependent on  $\eta_s$  as we shall see later.

A strong increase in viscosity occurs when the melt fraction equals 40% (Abe, 1997). Hence, when the melt fraction approaches this critical value, the presence of crystals drastically reduces the efficiency of the magma ocean cooling. In our models, the mantle is considered as part of the magma ocean as long as its melt fraction is larger than 50% (Neumann et al., 2014) and we stop our simulations when the thickness of the magma ocean drop below 100 km.

The pressure profile  $P$  is obtained fitting the PREM model (Dziewonski and Anderson, 1981) with a quadratic function of the radius  $r$  and is assumed to remain constant with time:

$$P = 4.0074 \times 10^{11} - 91862r + 0.0045483r^2. \quad (9)$$

## 2.2. Melting curves and adiabats

Due to the uncertainties related to the chemical composition of the magma ocean, we consider in our study two models for melting curves and elastic parameters: the F-peridotite model and the A-chondritic model. We describe these two models in the following sections.

### 2.2.1. Melting curves

The solidus and liquidus play a major role in the early thermal evolution of the magma ocean. Recent laboratory experiments now constrain the liquidus and solidus of mantle-like material up to pressures compatible with the CMB conditions (Fiquet et al., 2010; Andraut et al., 2011). However, the differences between these two studies, in particular the liquidus temperatures, appear too large to be solely due to the difference in chemical compositions between the two types of mantle materials. Regardless of the controversy, we performed calculations using the melting curves from both reports, leading to a F-peridotitic model (Fiquet et al., 2010) and a A-chondritic model (Andraut et al., 2011). The solidus and liquidus profiles are obtained fitting experimental results with a modified Simon and Glatzel equation (Simon and Glatzel, 1929). For pressures below  $P = 20$  GPa, we use experimentally determined solidus and liquidus temperatures of chondritic mantle from Herzberg and Zhang (1996):

$$T_{sol} = 1661.2 \left( \frac{P}{1.336 \times 10^9} + 1 \right)^{(1/7.437)}, \quad (10)$$

$$T_{liq} = 1982.1 \left( \frac{P}{6.594 \times 10^9} + 1 \right)^{(1/5.374)}, \quad (11)$$

with  $T_{liq}$  is the liquidus temperature and  $T_{sol}$  the solidus temperature.

Since the difference between the F-peridotitic and A-chondritic solidus for pressures larger than  $P = 20$  GPa is not large, we use the experimentally determined A-chondritic solidus from Andraut et al. (2011):

$$T_{sol} = 2081.8 \left( \frac{P}{101.69 \times 10^9} + 1 \right)^{(1/1.226)}. \quad (12)$$

For pressures above 20 GPa, the difference between the F-peridotitic and the A-chondritic liquidus is more important. We use the following expression

$$T_{liq} = c_1 \left( \frac{P}{c_2} + 1 \right)^{(1/c_3)}, \quad (13)$$

with ( $c_1 = 78.74$ ,  $c_2 = 4.054 \times 10^6$ ,  $c_3 = 2.44$ ) for F-peridotitic liquidus (Fiquet et al., 2010) and ( $c_1 = 2006.8$ ,  $c_2 = 34.65 \times 10^9$ ,  $c_3 = 1.844$ ) for A-chondritic liquidus (Andraut et al., 2011).

### 2.2.2. Thermodynamical parameters

The thermodynamical parameters for the molten magma ocean are closely related to its chemical composition. Volume and elastic parameters of silicate liquids has been recently characterized up to 140 GPa using shock compression experiments (Mosenfelder et al., 2007, 2009; Thomas et al., 2012; Thomas and Asimow, 2013). We assume here two multicomponent systems for (i) a A-chondritic composition (62% enstatite + 24% forsterite + 8% fayalite + 4% anorthite + 2% diopside) and (ii) a F-peridotitic composition (33% enstatite + 56% forsterite + 7% fayalite + 3% anorthite + 0.7% diopside). Using fourth-order Birch–Murnaghan/Mie–Grüneisen equation of state fits for molten silicate liquids from Thomas and Asimow (2013), we obtain the melt density  $\rho_m$ , the volumetric thermal expansion  $\alpha$  as a function of pressure as well as the specific heat  $C_p$  of the molten material for these two multicomponent assemblages. The density of the solid phase is then calculated as:

$$\rho_s = \rho_m + \Delta\rho, \quad (14)$$

with  $\Delta\rho$  the density difference between solid and liquid (see Tables 1 and 2 for values).

**Table 1**

Constant and fixed parameter values for numerical models.

|                          |                   |                                                |
|--------------------------|-------------------|------------------------------------------------|
| Earth radius             | $R$               | 6370 km                                        |
| Core radius              | $R_{core}$        | 3470 km                                        |
| Mantle thickness         | $R - R_{core}$    | 2900 km                                        |
| <i>Mantle properties</i> |                   |                                                |
| Solid density            | $\rho_s$          | $= \rho_m + \Delta\rho$                        |
| Density contrast         | $\Delta\rho/\rho$ | 1.5% (Tosi et al., 2013)                       |
| Specific enthalpy change | $\Delta H$        | $4 \times 10^5$ J/kg (Ghosh and McSween, 1998) |
| Viscosity of melt phase  | $\eta_m$          | $1-10^4$ Pa s                                  |
| Bottom TBL thickness     | $e_{TBL}$         | $10^{-3}-10^3$ m                               |
| <i>Core properties</i>   |                   |                                                |
| Density                  | $\rho_{Fe}$       | $10\,000$ kg m $^{-3}$                         |
| Heat capacity            | $C_{p,Fe}$        | $800$ J kg $^{-1}$ K $^{-1}$                   |

For a zone of partial melting, the density  $\rho'$ , the coefficient of volumetric thermal expansion  $\alpha'$  and the specific heat  $C'_p$  are given as follows (Solomatov, 2007):

$$\frac{1}{\rho'} = \frac{1-\phi}{\rho_s} + \frac{\phi}{\rho_m}, \quad (15)$$

$$\alpha' = \alpha + \frac{\Delta\rho}{\rho(T_{liq} - T_{sol})}, \quad (16)$$

$$C'_p = C_p + \frac{\Delta H}{T_{liq} - T_{sol}}, \quad (17)$$

where  $\Delta H$  is the latent heat released during solidification.

### 2.2.3. Adiabats

In vigorously convecting systems such as magma oceans, the temperature distribution is nearly adiabatic and isentropic (Solomatov, 2007). In one-phase systems, such as a completely molten or a completely solid layer, the equation for an adiabat is

$$\left( \frac{\partial T}{\partial r} \right)_s = - \frac{\alpha g}{C_p} T. \quad (18)$$

In two-phase systems, the effects of phase changes need to be considered (Solomatov, 2007). The equation for such adiabat is given by:

$$\left( \frac{\partial T}{\partial r} \right)_s = - \frac{\alpha' g}{C'_p} T. \quad (19)$$

This leads to a two-phase adiabat that is steeper than the purely liquid or solid one-phase adiabats (Solomatov, 2007). The adiabatic temperature profiles are calculated by numerical integration of Eq. (18) and Eq. (19) using a fourth-order Runge–Kutta method (Press et al., 1993). These adiabatic temperature profiles are used to calculate at each depth and, when super-adiabatic, the temperature difference  $\Delta T$  from Eq. (3). The liquidus and solidus profiles as well as the adiabatic profiles obtained from Eq. (18) for temperatures ranging between 1400 and 4000 K are shown in Fig. 1. We start our models assuming an adiabatic temperature profile with a potential surface temperature  $T_p = 3200$  K.

### 2.3. Boundary conditions

Large impacts can generate a rock vapor atmosphere that can last for some years until its energy is radiated to space (Svetsov, 2005). The presence of an atmosphere is expected to slow down the radiation of heat to space (Hamano et al., 2013; Lebrun et al., 2013). However, most of the pre-impact atmosphere is likely to be eroded after a giant impact (Shuvalov, 2009). Thus, in our models,

**Table 2**  
Variable and non-dimensional parameter values for numerical models.

|                               |          |                                                                                                                                            |                                                           |
|-------------------------------|----------|--------------------------------------------------------------------------------------------------------------------------------------------|-----------------------------------------------------------|
| Melt density                  | $\rho_m$ | A-model: 2684–5274 kg m <sup>-3</sup><br>F-model: 2679 – 5378 kg m <sup>-3</sup>                                                           | Computed from Thomas and Asimow (2013)                    |
| Heat capacity                 | $C_p$    | A-model: 1742 J kg <sup>-1</sup> K <sup>-1</sup><br>F-model: 1800 J kg <sup>-1</sup> K <sup>-1</sup>                                       | Computed from Thomas and Asimow (2013)                    |
| Thermal expansion coefficient | $\alpha$ | A-model: $1.3 \times 10^{-5}$ – $7.9 \times 10^{-5}$ K <sup>-1</sup><br>F-model: $2 \times 10^{-5}$ – $9.6 \times 10^{-5}$ K <sup>-1</sup> | Computed from Thomas and Asimow (2013)                    |
| Viscosity of solid phase      | $\eta_s$ |                                                                                                                                            | From Eq. (8) with $\eta_{s,0} = 256$ Pa s and $B = 25.17$ |
| Viscosity of the magma ocean  | $\eta$   | $1\text{--}10^{21}$ Pa s                                                                                                                   | From Eq. (7)                                              |
| Total conductivity            | $k$      | $5\text{--}10^7$ W m <sup>-1</sup> K <sup>-1</sup>                                                                                         | $= k_c + k_v$                                             |
| Rayleigh number               | $Ra$     | at $t = 0$ : $1 \times 10^{27}$ – $3 \times 10^{27}$                                                                                       | Computed from Eq. (3)                                     |
| Prandtl number                | $Pr$     | $350\text{--}3.6 \times 10^{24}$                                                                                                           | $= C_p \eta / k_c$                                        |
| Reynolds number               | $Re$     | at $t = 0$ : $Re \sim 10^9$                                                                                                                | From Solomatov (2007)                                     |

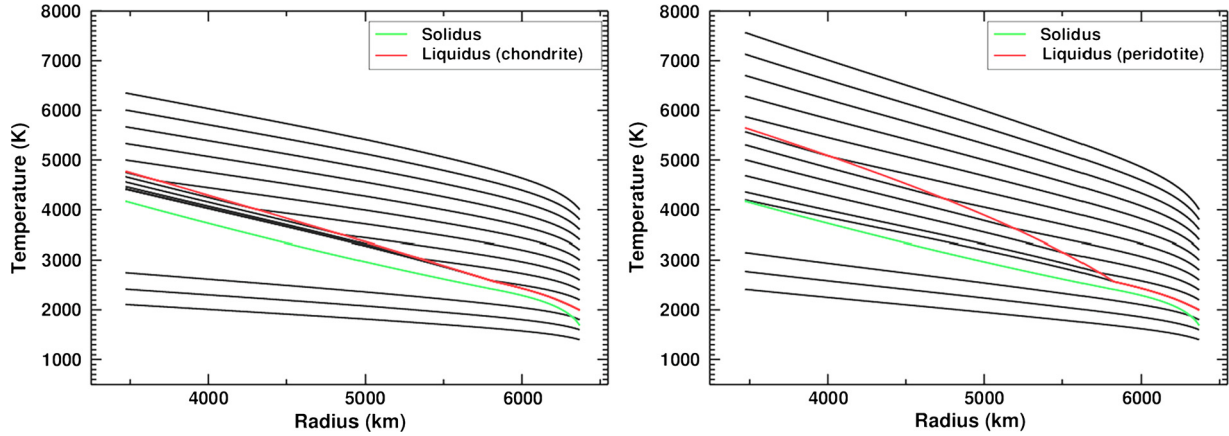


**Fig. 1.** Adiabats (with  $T_p$  ranging between 1400 and 4000 K) computed for the A-chondritic model (left) and the F-peridotitic model (right). The corresponding solidus and liquidus are represented in green and red respectively. (For interpretation of the references to color in this figure legend, the reader is referred to the web version of this article.)

we neglect the effect of thermal blanketing, and impose a radiative heat flux boundary condition at the surface:

$$F_{surf} = \sigma (T_{surf}^4 - T_{eq}^4), \quad (20)$$

with  $T_{surf}$  the temperature at the surface of the MO,  $\sigma$  the Stefan-Boltzman constant and  $T_{eq} = 273$  K the expected equilibrium surface temperature.

At the base of the silicate mantle, core–mantle thermal coupling is accounted for via a conductive heat flux imposed at the core–mantle boundary (CMB):

$$F_{core} = \frac{k_c (T_{core} - T_{CMB}^{mantle})}{e_{TBL}}, \quad (21)$$

where  $T_{core}$  is the average core temperature at the CMB (i.e. we neglect the thermal boundary layer within the core) and  $T_{CMB}^{mantle}$  is the mantle temperature right above the CMB.  $e_{TBL}$  is the thickness of the thermal boundary layer at the bottom of the mantle where the heat is extracted from the core by conduction.  $T_{CMB}^{mantle}$  is obtained solving Eq. (1) while  $T_{core}$  is obtained from:

$$V_{core} \rho_{Fe} C_{p,Fe} \frac{dT_{core}}{dt} = S_{core} F_{core}, \quad (22)$$

where  $V_{core}$  is the core volume,  $S_{core}$  is the core surface,  $\rho_{Fe}$  is the core density,  $C_{p,Fe}$  is the core heat capacity and  $F_{core}$  is the heat flux through the CMB. This formulation allows to follow the evolution of core temperature as a function of time, based on the CMB heat flux.

#### 2.4. Numerical model

Eq. (1) is discretized using a semi-implicit predictor–corrector Finite Difference scheme, of second-order in both space and time

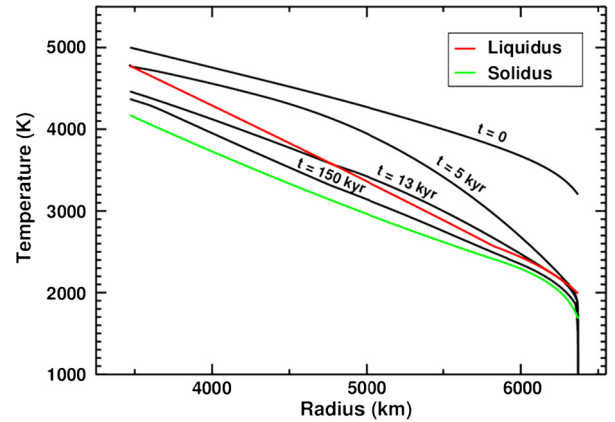


**Fig. 2.** Temperature evolution from an initially adiabatic temperature profile with  $T_p = 3200$  K and  $T_0^{core} = 5000$  K. The liquidus and solidus used in our models are those obtained for the A-chondritic model and are represented respectively with red and green curves. In this model  $e_{TBL} = 1$  m and  $\eta_m = 100$  Pa s. (For interpretation of the references to color in this figure legend, the reader is referred to the web version of this article.)

(Press et al., 1993). Our scheme was successfully benchmarked against steady and unsteady analytical solutions for diffusion problems (Crank, 1975). The mantle is discretized using  $n = 2900$  equally spaced grid points resulting in a constant spatial resolution  $\Delta r = 1$  km. Non-linear effects are handled via a fixed-point/pi-card iteration procedure. The variable time step is determined as  $\Delta t = \min(\Delta r^2 / \kappa)$ , where  $\kappa(r) = k / (\rho C_p)$  is the effective diffusivity.

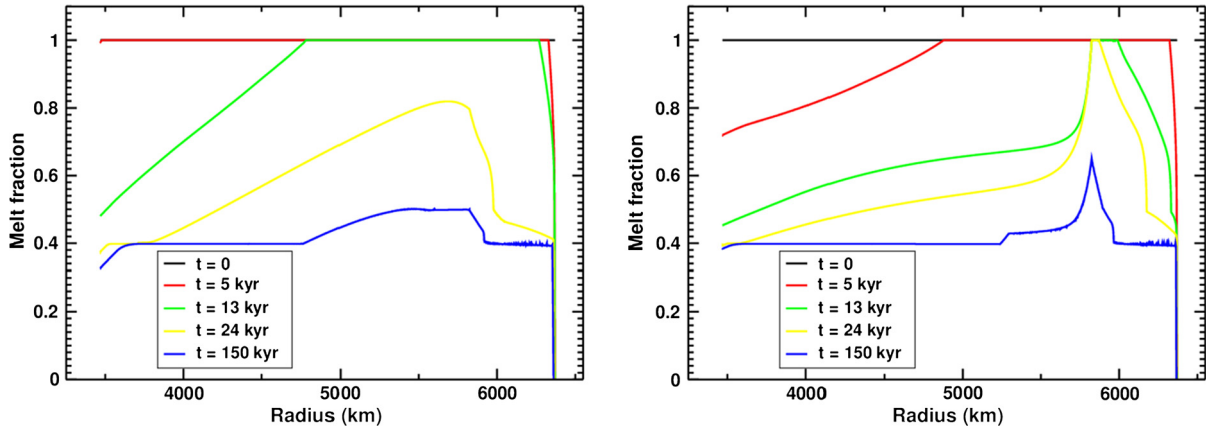


**Fig. 3.** **Left panel:** Melt fraction evolution from an initially completely molten magma ocean and corresponding to the case illustrated in Fig. 2. A melt fraction of 0.4 is a major discontinuity for the magma ocean viscosity (see text). **Right panel:** same with a F-peridotitic model and  $T_0^{core} = 7000$  K.

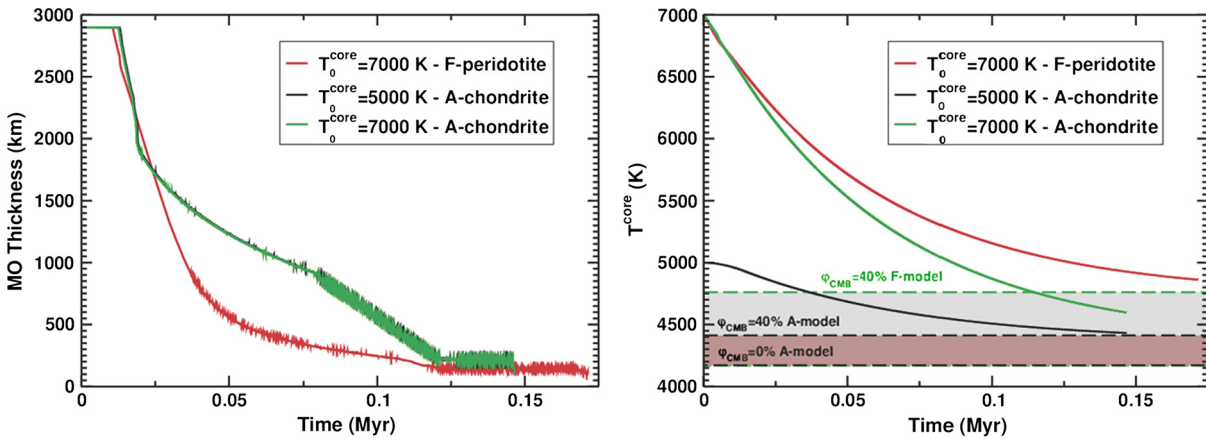


**Fig. 4.** **Left panel:** Time evolution of the magma ocean thickness (where the melt fraction is larger than 50%) for different initial core temperatures  $T_0^{core}$  and different initial compositions (with  $e_{TBL} = 1$  m and  $\eta_m = 100$  Pa s). **Right panel:** Time evolution of the core temperature for different initial core temperatures and different initial compositions (with  $e_{TBL} = 1$  m,  $\eta_m = 100$  Pa s). (For interpretation of the references to color in this figure legend, the reader is referred to the web version of this article.)

### 3. Results

#### 3.1. Thermal evolution of a deep magma ocean

We follow the thermal evolution of a deep magma ocean with an initially adiabatic temperature profile with  $T_p = 3200$  K. Before we study the effect of each magma ocean parameter, we consider the following model as a reference case: a A-chondritic model, a 1 m thick bottom thermal boundary layer ( $e_{TBL}$ ), a melt viscosity value of  $\eta_m = 100$  Pa s and an initial core temperature  $T_0^{core} = 5000$  K. Fig. 2 shows that the temperature rapidly decreases from the surface where heat is efficiently removed by radiative cooling even if a thin solid crust is formed within this upper thermal boundary layer. In the deepest part of the mantle, the temperature profile remains adiabatic but the cooling is slower. After 5000 yr, solidification occurs from the CMB where the liquidus is steeper than the adiabatic profile. As cooling proceeds, the melt fraction decreases and the last parcel with 100% melt starts to solidify in the upper mantle (see Fig. 3, left). Finally, the whole magma ocean drops below a 50% melt value in  $t_{MO} \sim 150$  kyr with  $t_{MO}$  being the magma ocean lifetime. This time ranges between the two characteristic timescales mentioned in Solomatov (2000):  $10^3$  yr when crystallization starts from the bottom and  $10^8$  yr when crystallization of the last drop of melt occurs in the shallow magma ocean. Clearly, our magma ocean lifetime is much shorter than the cooling timescale of  $\sim 4$  Gyr proposed by Labrosse et al. (2007). This is due to the fact that, in our model, the solidification occurs from

the bottom-up which prevents our magma ocean from being overlaid by a thick insulating solid mantle. In Abe (1997), the magma ocean was restricted to a 1000 km-deep domain and the melting curves were steeper than the one used in our model. Hence, within 150 kyr, most of the mantle temperature profile computed from Abe (1997) is well below the solidus.

We monitored the thickness of the magma ocean (i.e. the thickness of the material having a melt fraction larger than 50%) as a function of time. Fig. 4 (left, black line) shows that after a short period ( $\sim 20$  kyr) where the mantle remains mostly molten, the thickness of the magma ocean rapidly decreases from 2900 km to 200 km, with a change of slope for a thickness of  $\sim 2000$  km for the A-chondritic model. At the change of slope, the melt fraction reaches the critical value of 40% in the lowermost mantle, which induces an abrupt increase of its viscosity. Then the melt fraction progressively decreases at all mantle depths until we stop our simulations when the magma ocean thickness drops below 100 km. Fig. 4 (right, black line) shows the core temperature as a function of time for our reference case. In this model, the core temperature decreases monotonically from its initial value of 5000 K to a value of 4430 K, which corresponds to a melt fraction  $\phi \sim 40\%$  at  $P = 140$  GPa (i.e. when the abrupt change in viscosity occurs).

We monitored the time evolution of the heat flow coming at the CMB from the core  $F_{core}$  and the heat loss at the surface  $F_{surf}$  (Fig. 5, a). During the first 20 kyr, the heat flow at the CMB rapidly increases from  $\sim 10^{16}$  to a nearly constant value of  $\sim 10^{17}$  W. In the meantime the surface heat flow decreases from

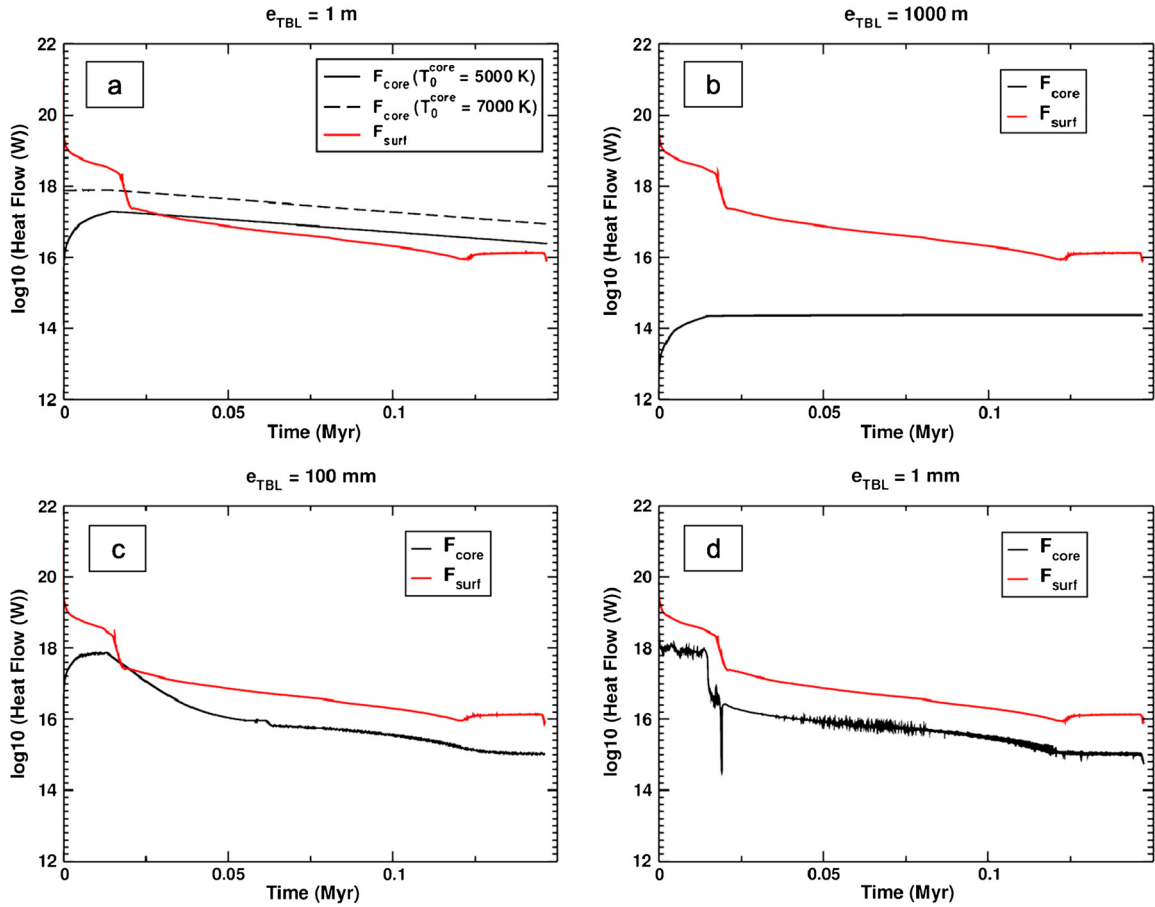


**Fig. 5.** (a): Time evolution of the CMB (black) and surface (red) heat flows for a A-chondritic model (assuming  $e_{TBL} = 1$  m,  $\eta_m = 100$  Pa s and  $T_0^{core} = 5000$  K except for the black dashed line where  $T_0^{core} = 7000$  K). (b): Same with  $e_{TBL} = 1000$  m. (c): Same with  $e_{TBL} = 100$  mm. (d): Same with  $e_{TBL} = 1$  mm. In all these models, the magma ocean lifetimes (time at which the plots ends up) are very close. (For interpretation of the references to color in this figure legend, the reader is referred to the web version of this article.)

$\sim 10^{19}$  (in agreement with the value proposed by Solomatov, 2000) to  $\sim 10^{17}$  W. Then, both the surface and the core heat flows decrease down to a value of  $\sim 10^{16}$  W until the end of the magma ocean stage (within  $t_{MO} = 150$  kyr).

### 3.2. Influence initial of core temperature

We monitored the influence of the initial core temperature on the cooling of the deep magma ocean considering two values: (1)  $T_0^{core} = 5000$  K, which is equal to the temperature at the bottom of the magma ocean for  $T_p = 3200$  K in the A-chondritic model and (2)  $T_0^{core} = 7000$  K, which corresponds to a core significantly hotter than the mantle. The comparison of the black and green curves in Fig. 4 (left) shows that the initial temperature has a negligible influence on the evolution of the magma ocean thickness as well as on its cooling timescale. When  $T_0^{core} = 7000$  K, the initial core heat flow is large ( $\sim 10^{18}$  W) (Fig. 5, a) because of the initial temperature contrast ( $= 2000$  K) with the lowermost mantle. Then the heat flow decreases as a consequence of both the progressive solidification of the overlying mantle and the core heat depletion. When  $T_0^{core} = 5000$  K, the initial CMB heat flow is much smaller than when  $T_0^{core} = 7000$  K, but it increases rapidly due to rapid cooling of the lowermost mantle. In both cases, the heat flow decreases when the lowermost mantle has cooled sufficiently to reach the critical melt fraction of 40%. A significantly hotter initial core leads to an increase of the core heat flow, by a factor of 3 between 5000 K and 7000 K (Fig. 5, a). However, this increase of the initial core temperature, which should lead to an increase of the

surface heat flow, is not visible on the surface heat flow evolution because of the stronger efficiency of the surface cooling.

Also, a core initially 2000 K hotter than the lowermost mantle ends up 170 K hotter at the end of the MO stage (Fig. 4, right). When  $T_0^{core} = 7000$  K the final core temperature is  $T^{core} = 4600$  K which is slightly larger than the temperature at which the melt fraction of the lowermost mantle reaches the 40% critical value in the A-chondritic model.

### 3.3. A-chondritic vs. F-peridotitic model

Here we compare the evolutions of temperature and melt fraction between the A-chondritic and F-peridotitic models (using the corresponding liquidus and thermodynamical parameters). We focus on cases where  $T_0^{core} = 7000$  K (with  $T_0^{core} = 5000$  K, the core temperature would be lower than the liquidus for the F-peridotitic model at the CMB pressure). Fig. 4 (left) shows that for an initial core temperature  $T_0^{core} = 7000$  K, the magma ocean thickness decreases more rapidly in the F-peridotitic model (red curve) than in the A-chondritic model (green curve). This is the direct consequence of a liquidus being significantly higher for a F-peridotitic model than for a A-chondritic model (Fig. 1). Hence, during the cooling of an initial fully molten magma ocean, the onset of mantle crystallization occurs earlier and the melt fraction decreases more rapidly in the F-peridotitic case (Fig. 3, right). The comparison of the A-chondritic and the F-peridotitic models shows a peak of the melt fraction in the latter case occurring at a depth of  $\sim 600$  km. This corresponds to the important slope change in the F-peridotitic liquidus that occurs at 20 GPa (see Fig. 1, right). Since the melt

fraction is a strong function of the liquidus, this discontinuity happens to affect the precise depth at which the last drop of melt should solidify. However, the last part to solidify should still be located in the shallow mantle, regardless the shape of the liquidus in this region. In addition, the magma ocean lifetime  $t_{MO}$  appears to be weakly affected by the choice of the model and ranges between 147 kyr (in the A-chondritic case) to 171 kyr (in the F-peridotitic case).

Still, the F-peridotitic and A-chondritic models show a significant difference on the evolution of the core temperature (Fig. 4, right). For both cases, the core temperature decreases asymptotically from its initial value to a value that ranges between 4600 K (A-chondritic case) and 4860 K (F-peridotitic) in about 0.15 Myr. Since the lowermost mantle solidifies more rapidly when considering a hotter liquidus, a F-peridotitic model for the magma ocean helps to retain some heat in the core. For both cases, the final core temperature is 100 to 150 K larger than the temperature at which the melt fraction of the lowermost mantle reaches the 40% critical value.

### 3.4. Influence of the bottom thermal boundary layer

The thickness of the bottom thermal boundary layer  $e_{TBL}$  governs both the cooling rate of the core and the energy supplied to the magma ocean (Eq. (21)). In a hard-turbulent context, this thickness is difficult to determine from laboratory experiments and only theoretical models can constrain this parameter (Spiegel, 1971). Therefore, a rough estimation of  $e_{TBL}$  can be obtained for  $Ra \sim 10^{20}$  based on the Nusselt number calculation:  $Nu \sim (RaPr)^{1/2}$  (Spiegel, 1971). Considering that  $Nu \sim L/e_{TBL}$ , we obtain  $e_{TBL} \sim L(RaPr)^{-1/2}$ . In our magma ocean context and assuming that the scaling law is still valid at Rayleigh numbers up to  $10^{30}$ , this corresponds to a value  $e_{TBL} \sim 10^{-6}$  m. This thickness is extremely thin, however, it is compatible with previous reports (Solomatov, 2007; Lebrun et al., 2013). As a first attempt to understand the influence of bottom thermal boundary layer in the magma ocean cooling dynamics, we performed various calculations with  $e_{TBL}$  fixed and ranging from 1 mm to 1 km. The lower range values can be seen as unrealistic in comparison with, for example, the core topography. However, the wide range of values considered for  $e_{TBL}$  allows a better illustration of its influence on the magma ocean cooling timescales.

We find that the magma ocean lifetime does not depend largely on  $e_{TBL}$  and its value remains close to 150 kyr for the whole range of  $e_{TBL}$  values assumed here. Fig. 5 shows the CMB and the surface heat flows for four different values of  $e_{TBL}$ . For  $e_{TBL} = 1000$  m (Fig. 5, b), the surface heat flow is several orders of magnitude larger than the core heat flow and the thermal coupling between these two reservoirs is inefficient. For values of thermal boundary layer thicknesses below 1 m (Fig. 5, c and d), the heat flows become comparable and the thermal coupling between the core and the molten overlying mantle becomes efficient. Ideally,  $e_{TBL}$  should be an adjustable parameter in our calculation, related to the effective value of the Rayleigh number. However, this would result in extremely small  $e_{TBL}$  values of the order of  $10^{-6}$  m. We show in Fig. 5 that decreasing the value of  $e_{TBL}$  from 100 mm to a value of 1 mm does influence neither the shape of the surface heat flow nor the magma ocean lifetime (Fig. 5, c and d). In that cases, the core heat flow rapidly reaches a maximal value and decreases within the first 20 kyr, which corresponds to the time needed by the melt fraction of the bottom of the magma ocean to reach the critical value of 40% (Fig. 6). During this brief period of time, although heat is efficiently removed from the core (Fig. 6), the CMB heat flow remains considerably smaller than the surface heat loss. This is the reason why  $e_{TBL}$  does not significantly influence the magma ocean lifetime. Hence, decreasing  $e_{TBL}$  to a smaller value

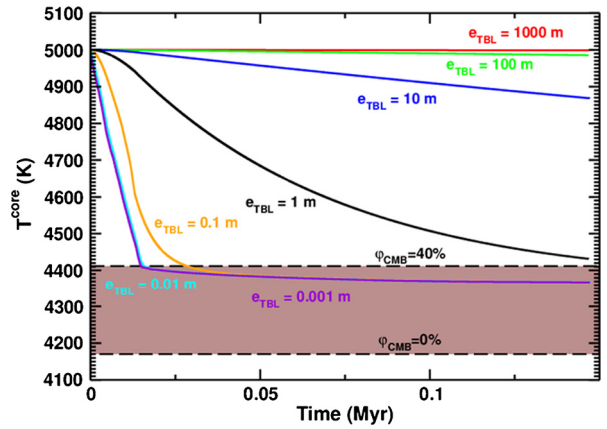


Fig. 6. Time evolution of the core temperature for different thicknesses of the bottom thermal boundary layer (assuming a A-chondritic model,  $\eta_m = 100$  Pa s and  $T_0^{core} = 5000$  K).

(i.e.  $e_{TBL} \ll 10^{-6}$  m) as suggested by our theoretical estimation of the TBL thickness or to relate  $e_{TBL}$  to the Rayleigh number that is initially extremely high should not influence the results of our study.

Such a behavior is confirmed by the time evolution of  $T^{core}$ , which is a strong function of  $e_{TBL}$  (Fig. 6). As long as  $e_{TBL}$  is larger than 100 m, the initial core heat is efficiently retained and the core cooling is not influenced by the cooling of the overlying magma ocean. However, for  $e_{TBL} \leq 100$  m the thermal coupling between the core and the MO becomes important. For  $e_{TBL} < 1$  m, the core rapidly cools down to  $\sim 4400$  K, which corresponds to the temperature where the lowermost mantle reaches the critical melt fraction value of 40%. Then the core cooling efficiency strongly decreases as the lowermost mantle is becoming much more viscous. Finally, the core temperature ends up at a temperature of  $\sim 4370$  K for  $e_{TBL}$  values ranging between 1 mm to 10 cm.

### 3.5. Influence of the magma ocean viscosity

Measurements (Liebske et al., 2005) and ab initio calculations (Karki and Stixrude, 2010) estimate that the dynamic viscosity  $\eta_m$  of peridotitic melt is in the range  $10^{-2}$ – $10^{-1}$  Pa s. At low degrees of partial melting of a peridotite, the viscosity of the generated liquid can eventually increase up to 100 Pa s (Kushiro, 1986). The viscosity of molten mafic silicate should range between  $10^{-2}$ – $10^2$  Pa s (Rubie et al., 2003). To take into account the effect of this uncertainty on the magma ocean lifetime, we perform numerical simulations considering that the fully molten magma ocean viscosity  $\eta_m$  ranges between  $10^{-2}$ – $10^2$  Pa s.

Dimensional analysis of Eq. (1) indicates that  $t_{MO}$  is inversely proportional to  $F_{conv}$ . In the hard turbulent regime relevant to a thick MO context this term scales as  $\eta_m^{-3/7}$ . Consequently, the lifetime of a magma ocean should scale as  $\eta_m^{3/7}$ . This is confirmed by our numerical results (Fig. 7), and consistent with previous work (Solomatov, 2007):

$$t_{MO}(\text{Myr}) = 0.018 \eta_m^{3/7}. \quad (23)$$

Most importantly, for realistic viscosities of the fully molten early mantle, the melt fraction drops below 50% at all mantle depths in less than 1 Myr. For the lower range of  $\eta_m$ , this characteristic time scale can decrease down to several kyrs, rather than 1 Myr.

## 4. Conclusion

The cooling of a thick terrestrial magma ocean is a fast process. The magma ocean lifetime is principally governed by its viscosity



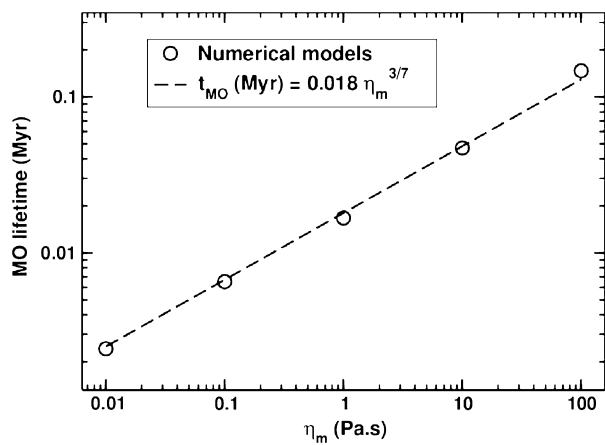


Fig. 7. Magma ocean lifetime as a function of the magma ocean viscosity  $\eta_m$  (assuming a A-chondritic model,  $e_{TBL} = 1$  m and  $T_0^{core} = 5000$  K).

and, for the mid range of realistic viscosities, the magma ocean reaches a 50% melt fraction at all mantle depths within 20 kyr. Depending on the thermal boundary layer at the CMB, the thermal coupling between the core and MO can either insulate the core during the MO solidification and favor a hot core (for thick TBL), or drain the heat out of the core. However, as suggested by theoretical calculations, an extremely thin thermal boundary layer in an ultra-turbulent environment implies that much of the heat is removed from the core during the cooling of the overlying mantle. In this context, our F-peridotitic model (with a higher liquidus) is more willing to retain the core heat than our A-chondritic model, yielding a difference of temperature of  $\sim 170$  K after the magma ocean has crystallized. In addition, the final core temperature increases by a couple hundred degrees as its early temperature increases. However, for all cases, the average core temperature at the CMB ( $T^{core}$ ) ends up close to the 40% melt fraction temperature of the silicate magma ocean:  $\pm 100$  K depending on the initial core temperature and on the thickness of the bottom thermal boundary layer.

In contrast with previous reports (Labrosse et al., 2007), our model shows that the crystallization occurs relatively rapidly at the CMB and, after some crystallization has proceeded, the highest amount of partial melting is found at intermediate depth between the surface and the CMB (see Fig. 3). One could argue that this result is dictated by the fact that our calculation neglects the possible effects of chemical segregation during mantle cooling. On the contrary, we believe that the segregation of a melt above the core mantle boundary would not help to retain heat in the core (Labrosse, 2015; Davies et al., 2015). A melt that would accumulate just above the CMB by gravitational segregation would be depleted in refractory elements, thus with a liquidus lower than the rest of the mantle. The temperature at which this part of the mantle becomes viscous (at 40% of partial melting) would be lowered and thus the core heat would escape more easily in the presence of a basal magma ocean (Ulvrová et al., 2012; Nakagawa and Tackley, 2014), in agreement with our results displayed in Fig. 4.

These results have important consequences for the magnetic history of the Earth. Indeed, if at some point, a full magma ocean has existed on the Earth, it is likely that most of the core heat has been removed rapidly. In less than 1 Myr, a tremendous heat flow may have led to a significant decrease of the core temperature until it reached a value that is close or slightly above the temperature at which the melt fraction of the lowermost mantle reaches the 40% critical value (i.e.  $\sim 4400$  K). Assuming that the Earth–Moon system was formed by a giant impact 100 Myrs after the first solids of the Solar System (Kleine and Rudge, 2011),

and that this giant impact has completely molten the Earth's mantle (Nakajima and Stevenson, 2015), it is difficult to envision that a large amount of heat could be retained in the core to sustain the geomagnetic field by thermal convection for several Gyr (Andraut et al., 2016), in contrast with the proposition of the most recent reports (Labrosse, 2015; Davies et al., 2015).

Finally, we acknowledge that our current model neglects the effect of vertical chemical segregation. While this effect is unlikely to dominate the dynamics in a highly turbulent magma ocean (Tonks and Melosh, 1990), it could become more important when the degree of partial melting becomes close or lower than  $\sim 40\%$  (i.e. when viscosity increases). At this point, the knowledge of the density contrast between the solid at the liquidus (the first crystal to form) and the ambient liquid becomes of major importance. Whether the melt sinks, or floats has important ramifications for understanding the first steps in the dynamic modeling of the Earth's differentiation. In the near future, a modeling effort to integrate the compositional contribution in the buoyancy calculation between liquid and solid will constitute an important step forward towards the understanding of the earliest stages of Earth's evolution.

### Acknowledgements

The authors thank J. Roberts and anonymous reviewer for thoughtful and constructive comments. The authors also thank G. Tobie and B. Cecconi for their useful help in the development of the numerical model as well as M. Le Bars and J. Lunine for fruitful discussions and help. J. Monteux and D. Andraut are funded by Agence Nationale de la Recherche (Oxydeep decision no. ANR-13-BS06-0008). J. Monteux is also funded by the Auvergne Fellowship program. H. Samuel acknowledges the support from the Deutsche Forschungsgemeinschaft (project SA 2042/3). This is Laboratory of Excellence ClerVolc contribution no. 205.

### References

- Abe, Y., 1997. Thermal and chemical evolution of the terrestrial magma ocean. *Phys. Earth Planet. Inter.* 100, 27–39. [http://dx.doi.org/10.1016/S0031-9201\(96\)03229-3](http://dx.doi.org/10.1016/S0031-9201(96)03229-3).
- Agnor, C.B., Canup, R.M., Levison, H.F., 1999. On the character and consequences of large impacts in the late stage of terrestrial planet formation. *Icarus* 142, 219–237. <http://dx.doi.org/10.1006/icar.1999.6201>.
- Allègre, C.J., Poirier, J.-P., Humler, E., Hofmann, A.W., 1995. The chemical composition of the Earth. *Earth Planet. Sci. Lett.* 134, 515–526. [http://dx.doi.org/10.1016/0012-821X\(95\)00123-T](http://dx.doi.org/10.1016/0012-821X(95)00123-T).
- Andraut, D., Bolfan-Casanova, N., Nigro, G.L., Bouhifd, M.A., Garbarino, G., Mezouar, M., 2011. Solidus and liquidus profiles of chondritic mantle: implication for melting of the Earth across its history. *Earth Planet. Sci. Lett.* 304, 251–259. <http://dx.doi.org/10.1016/j.epsl.2011.02.006>.
- Andraut, D., Petitgirard, S., Lo Nigro, G., Devidal, J.-L., Veronesi, G., Garbarino, G., Mezouar, M., 2012. Solid-liquid iron partitioning in Earth's deep mantle. *Nature* 487, 354–357. <http://dx.doi.org/10.1038/nature11294>.
- Andraut, D., Monteux, J., Le Bars, M., Samuel, H., 2016. The deep Earth may not be cooling down. *Earth Planet. Sci. Lett.* 443, 195–203. <http://dx.doi.org/10.1016/j.epsl.2016.03.020>.
- Boyet, M., Carlson, R.W., 2005.  $^{142}\text{Nd}$  evidence for early ( $>4.53$  Ga) global differentiation of the silicate Earth. *Science* 309, 576–581. <http://dx.doi.org/10.1126/science.1113634>.
- Canup, R.M., 2012. Forming a Moon with an Earth-like composition via a giant impact. *Science* 338, 1052. <http://dx.doi.org/10.1126/science.1226073>.
- Carlson, R.W., Lugmair, G.W., 2000. Timescales of Planetsimal Formation and Differentiation Based on Extinct and Extant Radioisotopes. *Ariz. Univ. Press, Tucson*, pp. 25–44.
- Crank, J., 1975. *The Mathematics of Diffusion*, 2nd ed. Clarendon Press, Oxford. viii, 414 p.
- Čuk, M., Stewart, S.T., 2012. Making the Moon from a fast-spinning Earth: a giant impact followed by resonant despinning. *Science* 338, 1047. <http://dx.doi.org/10.1126/science.1225542>.
- Davies, C., Pozzo, M., Gubbins, D., Alfè, D., 2015. Constraints from material properties on the dynamics and evolution of Earth's core. *Nat. Geosci.* 8, 678–685. <http://dx.doi.org/10.1038/ngeo2492>.

- Dziewonski, A.M., Anderson, D.L., 1981. Preliminary reference Earth model. *Phys. Earth Planet. Inter.* 25, 297–356. [http://dx.doi.org/10.1016/0031-9201\(81\)90046-7](http://dx.doi.org/10.1016/0031-9201(81)90046-7).
- Elkins-Tanton, L.T., Parmentier, E.M., Hess, P.C., 2003. Magma ocean fractional crystallization and cumulate overturn in terrestrial planets: implications for Mars. *Meteorit. Planet. Sci.* 38, 1753–1771.
- Elkins-Tanton, L.T., Zaranek, S.E., Parmentier, E.M., Hess, P.C., 2005. Early magnetic field and magmatic activity on Mars from magma ocean cumulate overturn. *Earth Planet. Sci. Lett.* 236, 1–12.
- Fiquet, G., Auzende, A.L., Siebert, J., Corgne, A., Bureau, H., Ozawa, H., Garbarino, G., 2010. Melting of peridotite to 140 gigapascals. *Science* 329, 1516. <http://dx.doi.org/10.1126/science.1192448>.
- Ghosh, A., McSween, H.Y., 1998. A thermal model for the differentiation of asteroid 4 Vesta, based on radiogenic heating. *Icarus* 134, 187–206. <http://dx.doi.org/10.1006/icar.1998.5956>.
- Hamano, K., Abe, Y., Genda, H., 2013. Emergence of two types of terrestrial planet on solidification of magma ocean. *Nature* 497, 607–610. <http://dx.doi.org/10.1038/nature12163>.
- Herzberg, C., Zhang, J., 1996. Melting experiments on anhydrous peridotite k1b-1: compositions of magmas in the upper mantle and transition zone. *J. Geophys. Res.*, Solid Earth 101 (B4), 8271–8295. <http://dx.doi.org/10.1029/96JB00170>.
- Javoy, M., Kaminski, E., Guyot, F., Andraut, D., Sanloup, C., Moreira, M., Labrosse, S., Jambon, A., Agrinier, P., Davaille, A., Jaupart, C., 2010. The chemical composition of the Earth: enstatite chondrite models. *Earth Planet. Sci. Lett.* 293, 259–268. <http://dx.doi.org/10.1016/j.epsl.2010.02.033>.
- Karato, S.-I., Wu, P., 1993. Rheology of the upper mantle – a synthesis. *Science* 260, 771–778. <http://dx.doi.org/10.1126/science.260.5109.771>.
- Karki, B.B., Stixrude, L.P., 2010. Viscosity of MgSiO<sub>3</sub> liquid at Earth's mantle conditions: implications for an Early magma ocean. *Science* 328, 740. <http://dx.doi.org/10.1126/science.1188327>.
- Kaula, W.M., 1979. Thermal evolution of Earth and Moon growing by planetesimal impacts. *J. Geophys. Res.* 84, 999–1008.
- Ke, Y., Solomatov, V.S., 2009. Coupled core–mantle thermal evolution of early Mars. *J. Geophys. Res., Planets* 114 (13), 1–12.
- Kleine, T., Rudge, J.F., 2011. Chronometry of meteorites and the formation of the Earth and Moon. *Elements* 7, 41–46. <http://dx.doi.org/10.1016/j.gca.2006.06.004>.
- Kleine, T., Touboul, M., Bourdon, B., Nimmo, F., Mezger, K., Palme, H., Jacobsen, S.B., Yin, Q.-Z., Halliday, A.N., 2009. Hf–W chronology of the accretion and early evolution of asteroids and terrestrial planets. *Geochim. Cosmochim. Acta* 73, 5150–5188. <http://dx.doi.org/10.1016/j.gca.2008.11.047>.
- Kushiro, I., 1986. Viscosity of partial melts in the upper mantle. *J. Geophys. Res.* 91, 9343–9350. <http://dx.doi.org/10.1029/JB091iB09p09343>.
- Labrosse, S., 2015. Thermal evolution of the core with a high thermal conductivity. *Phys. Earth Planet. Inter.* 247, 36–55. <http://dx.doi.org/10.1016/j.pepi.2015.02.002>.
- Labrosse, S., Hernlund, J.W., Coltice, N., 2007. A crystallizing dense magma ocean at the base of the Earth's mantle. *Nature* 450, 866–869. <http://dx.doi.org/10.1038/nature06355>.
- Lebrun, T., Massol, H., Chassefière, E., Davaille, A., Marcq, E., Sarda, P., Leblanc, F., Brandeis, G., 2013. Thermal evolution of an early magma ocean in interaction with the atmosphere. *J. Geophys. Res., Planets* 118, 1155–1176. <http://dx.doi.org/10.1002/jgre.20068>.
- Liebske, C., Schmickler, B., Terasaki, H., Poe, B.T., Suzuki, A., Funakoshi, K.-i., Ando, R., Rubie, D.C., 2005. Viscosity of peridotite liquid up to 13 GPa: implications for magma ocean viscosities [rapid communication]. *Earth Planet. Sci. Lett.* 240, 589–604. <http://dx.doi.org/10.1016/j.epsl.2005.10.004>.
- Martin, H., Moya, J.-F., Guitreau, M., Blichert-Toft, J., Le Pennec, J.-L., 2014. Why Archaean TTG cannot be generated by MORB melting in subduction zones. *Lithos* 198, 1–13. <http://dx.doi.org/10.1016/j.lithos.2014.02.017>.
- Miller, G.H., Stolper, E.M., Ahrens, T.J., 1991. The equation of state of a molten komatiite: 2. Application to komatiite petrogenesis and the Hadean Mantle. *J. Geophys. Res.* 96, 11,849. <http://dx.doi.org/10.1029/91JB01203>.
- Monteux, J., Ricard, Y., Coltice, N., Dubuffet, F., Ulvrova, M., 2009. A model of metal–silicate separation on growing planets. *Earth Planet. Sci. Lett.* 287, 353–362.
- Monteux, J., Jellinek, A.M., Johnson, C.L., 2011. Why might planets and moons have early dynamos? *Earth Planet. Sci. Lett.* 310, 349–359. <http://dx.doi.org/10.1016/j.epsl.2011.08.014>.
- Mosenfelder, J.L., Asimow, P.D., Ahrens, T.J., 2007. Thermodynamic properties of Mg<sub>2</sub>SiO<sub>4</sub> liquid at ultra-high pressures from shock measurements to 200 GPa on forsterite and wadsleyite. *J. Geophys. Res., Solid Earth* 112, B06208. <http://dx.doi.org/10.1029/2006JB004364>.
- Mosenfelder, J.L., Asimow, P.D., Frost, D.J., Rubie, D.C., Ahrens, T.J., 2009. The MgSiO<sub>3</sub> system at high pressure: thermodynamic properties of perovskite, postperovskite, and melt from global inversion of shock and static compression data. *J. Geophys. Res., Solid Earth* 114, B01203. <http://dx.doi.org/10.1029/2008JB005900>.
- Moya, J.-F., Martin, H., 2012. Forty years of TTG research. *Lithos* 148, 312–336. <http://dx.doi.org/10.1016/j.lithos.2012.06.010>.
- Nakagawa, T., Tackley, P.J., 2014. Influence of combined primordial layering and recycled MORB on the coupled thermal evolution of Earth's mantle and core. *Geochim. Geophys. Geosyst.* 15, 619–633. <http://dx.doi.org/10.1002/2013GC005128>.
- Nakajima, M., Stevenson, D.J., 2015. Melting and mixing states of the Earth's mantle after the Moon-forming impact. *Earth Planet. Sci. Lett.* 427, 286–295. <http://dx.doi.org/10.1016/j.epsl.2015.06.023>.
- Neumann, W., Breuer, D., Spohn, T., 2014. Differentiation of Vesta: implications for a shallow magma ocean. *Earth Planet. Sci. Lett.* 395, 267–280. <http://dx.doi.org/10.1016/j.epsl.2014.03.033>.
- Nomura, R., Ozawa, H., Tateno, S., Hirose, K., Hernlund, J., Muto, S., Ishii, H., Hiraoka, N., 2011. Spin crossover and iron-rich silicate melt in the Earth's deep mantle. *Nature* 473, 199–202. <http://dx.doi.org/10.1038/nature09940>.
- Press, W.H., Teukolsky, S.A., Vetterling, W.T., Flannery, B.P., 1993. *Numerical Recipes in FORTRAN the Art of Scientific Computing*, 2nd ed. Cambridge University Press, New York, NY, USA.
- Ricard, Y., Šrámek, O., Dubuffet, F., 2009. A multi-phase model of runaway core–mantle segregation in planetary embryos. *Earth Planet. Sci. Lett.* 284, 144–150.
- Ringwood, A.E., 1966. Chemical evolution of the terrestrial planets. *Geochim. Cosmochim. Acta* 30, 41–104. [http://dx.doi.org/10.1016/0016-7037\(66\)90090-1](http://dx.doi.org/10.1016/0016-7037(66)90090-1).
- Rizo, H., Boyet, M., Blichert-Toft, J., Rosing, M.T., 2013. Early mantle dynamics inferred from <sup>142</sup>Nd variations in Archean rocks from southwest Greenland. *Earth Planet. Sci. Lett.* 377, 324–335. <http://dx.doi.org/10.1016/j.epsl.2013.07.012>.
- Rubie, D.C., Melosh, H.J., Reid, J.E., Liebske, C., Righter, K., 2003. Mechanisms of metal–silicate equilibration in the terrestrial magma ocean. *Earth Planet. Sci. Lett.* 205, 239–255.
- Safronov, V.S., 1978. The heating of the earth during its formation. *Icarus* 33, 3–12. [http://dx.doi.org/10.1016/0019-1035\(78\)90019-2](http://dx.doi.org/10.1016/0019-1035(78)90019-2).
- Samuel, H., Tackley, P.J., Evonuk, M., 2010. Heat partitioning in terrestrial planets during core formation by negative diapirism. *Earth Planet. Sci. Lett.* 290, 13–19.
- Shuvalov, V., 2009. Atmospheric erosion induced by oblique impacts. *Meteorit. Planet. Sci.* 44, 1095–1105. <http://dx.doi.org/10.1111/j.1945-5100.2009.tb01209.x>.
- Simon, F., Glatzel, 1929. Fusion–pressure curve. *Z. Anorg. Allg. Chem.* 178, 309.
- Solomatov, V., 2007. *Magma Oceans and Primordial Mantle Differentiation*. Schubert, G. (Ed.), *Treatise of Geophysics*, vol. 9. Elsevier.
- Solomatov, V.S., 2000. Fluid dynamics of a terrestrial magma ocean. In: Canup, R.M., Righter, K., 69 collaborating authors (Eds.), *Origin of the Earth and Moon*. University of Arizona Press, Tucson, pp. 323–338.
- Spiegel, E.A., 1971. Convection in stars: I. Basic Boussinesq convection. *Annu. Rev. Astron. Astrophys.* 9, 323. <http://dx.doi.org/10.1146/annurev.aa.09.090171.001543>.
- Stixrude, L., de Koker, N., Sun, N., Mookherjee, M., Karki, B.B., 2009. Thermodynamics of silicate liquids in the deep Earth. *Earth Planet. Sci. Lett.* 278, 226–232. <http://dx.doi.org/10.1016/j.epsl.2008.12.006>.
- Svetsov, V.V., 2005. Numerical simulations of very large impacts on the Earth. *Planet. Space Sci.* 53, 1205–1220. <http://dx.doi.org/10.1016/j.pss.2005.04.011>.
- Tackley, P.J., 2012. Dynamics and evolution of the deep mantle resulting from thermal, chemical, phase and melting effects. *Earth-Sci. Rev.* 110, 1–25. <http://dx.doi.org/10.1016/j.earscirev.2011.10.001>.
- Thomas, C.W., Asimow, P.D., 2013. Direct shock compression experiments on pre-molten forsterite and progress toward a consistent high-pressure equation of state for CaO–MgO–Al<sub>2</sub>O<sub>3</sub>–SiO<sub>2</sub>–FeO liquids. *J. Geophys. Res., Solid Earth* 118, 5738–5752. <http://dx.doi.org/10.1002/jgrb.50374>.
- Thomas, C.W., Liu, Q., Agee, C.B., Asimow, P.D., Lange, R.A., 2012. Multi-technique equation of state for Fe<sub>2</sub>SiO<sub>4</sub> melt and the density of Fe-bearing silicate melts from 0 to 161 GPa. *J. Geophys. Res., Solid Earth* 117, B10206. <http://dx.doi.org/10.1029/2012JB009403>.
- Tonks, W.B., Melosh, H.J., 1990. *The Physics of Crystal Settling and Suspension in a Turbulent Magma Ocean*. Oxford University Press, pp. 151–174.
- Tonks, W.B., Melosh, H.J., 1992. Core formation by giant impacts. *Icarus* 100, 326–346.
- Tosi, N., Plesa, A.-C., Breuer, D., 2013. Overturn and evolution of a crystallized magma ocean: a numerical parameter study for Mars. *J. Geophys. Res., Planets* 118, 1512–1528. <http://dx.doi.org/10.1002/jgre.20109>.
- Touboul, M., Puchtel, I.S., Walker, R.J., 2012. W-182 evidence for long-term preservation of early mantle differentiation products. *Science* 335 (6072), 1065–1069. <http://dx.doi.org/10.1126/science.1216351>.
- Ulvrova, M., Labrosse, S., Coltice, N., Råback, P., Tackley, P.J., 2012. Numerical modelling of convection interacting with a melting and solidification front: application to the thermal evolution of the basal magma ocean. *Phys. Earth Planet. Inter.* 206, 51–66. <http://dx.doi.org/10.1016/j.pepi.2012.06.008>.
- Čížková, H., van den Berg, A.P., Spakman, W., Matyska, C., 2012. The viscosity of Earth's lower mantle inferred from sinking speed of subducted lithosphere. *Phys. Earth Planet. Inter.* 200, 56–62. <http://dx.doi.org/10.1016/j.pepi.2012.02.010>.
- Yoshino, T., Walter, M.J., Katsura, T., 2003. Core formation in planetesimals triggered by permeable flow. *Nature* 422, 154–157.